Electron states in random alloys with short-range order

Paul Bloom* and Daniel Mattis†
Belfer Graduate School of Science, Yeshiva University, New York, New York 10033
(Received 3 August 1976)

We present an accurate and economical iterative method of calculating the energy levels of a disordered or partly ordered random alloy. Results presented for one- and three-dimensional simple cubic lattices compare favorably with exact calculations. We also present the systematic effects of partial short-range order in three dimensions. A theory of the one-particle propagators is presented, and the theory of electrical conductivity is developed in the context of our new method. Our formulas satisfy the exact conservation laws.

I. INTRODUCTION

The study of electronic and vibrational spectra of disordered alloys is currently one of the principal concerns of solid-state physics,[1] stimulated by the outstanding successes of the coherent-potential approximation[2,3] (CPA), now ending its first decade. Although efforts to improve our understanding beyond the CPA have not all met with the same good fortune, there have been recent exceptions. Cluster methods[4,5] have been devised which are accurate enough to reproduce the "peaky" structure of the density of states $\rho(\omega)$, which they sometimes do (notably in one dimension[4]) with startling fidelity. We have been working along such a cluster-type approach, and have found an extremely simple method translating directly into a computer algorithm. While unsuited to the theoretical study of Lifshitz[6] tails, our method has permitted us to reproduce many of the other known results over the theoretically permitted range of energy,[7] even near the energy maxima and minima, and additionally, permitted to study of the effect of short-range order. Along with Lifshitz, we envisage tails in $\rho(\omega)$ at the energy maxima and minima as arising from accidental correlations in increasingly large clusters, of a size that for practical reasons we are not at present capable of handling; however, the simplicity of the present method may suggest a natural extension to cover this.[8]

The basic outline of our paper is as follows: In Sec. II we present a method for the calculation of the single-body Green's function in the presence of an arbitrary number of impurities. We then discuss how our procedure can be implemented by the use of a convergence factor Σ. Section III is devoted to an analysis of the meaning and uses of the complex self-energy Σ within the context of a disordered medium. Results from our method are presented in Sec. IV, including the effects of short-range order. Beyond this in Sec. V we make further approximations that allow us to determine $\bar{G}_{\vec{k}\vec{k}}(\omega)$. Section VI is concerned with the development of a transport theory compatible with $\bar{G}$, along the lines of Baym and Kadanoff.[9]

II. CLUSTER GREEN'S FUNCTION

Let the Hamiltonian for the electrons within a single tight-binding band in a hypercubic lattice in D dimensions be

$$H=\sum_{i,j} T_{ij}\,|i\rangle\langle j\,|+\sum_i V_i\,|i\rangle\langle i\,|\equiv T+V\,, \qquad (1)$$

with $T_{ij}=(2D)^{-1}$ for i,j nearest neighbors and zero otherwise, $|i\rangle$ the Wannier state at the lattice point R_i, and V_i the potential which takes on one of two values depending whether atom A or B occupies the i site. We construct the resolvent operator $G(z)$ and its various matrix elements:

$$G(z)\equiv(z-H)^{-1}=[\,z-(T+\Sigma)-(V-\Sigma)\,]^{-1}\,, \qquad (2)$$

in which we reference the operators to a complex "optical potential" $\Sigma(z)$ merely as a device to enhance the convergence of subsequent expansions, with z equal to the frequency ω, extended to the complex plane.

For those readers familiar with the CPA, it is important to note that our new departure consists principally in dissociating the complex self-energy parameter $\Sigma(\omega)$ from the site-diagonal averaged Green's function $\bar{G}_{nn}(\omega)$. Whereas in CPA, knowledge of the one implies the other, via the relationship

$$\bar{G}_{nn_{\rm CPA}}(z)=\langle n\,|\,\{z-[\,T+\Sigma_{\rm CPA}(z)\,]\}^{-1}|n\rangle\,, \qquad (3)$$

our experience indicates that it is better to treat $\Sigma(\omega)$ merely as a convergence parameter, one to be chosen as an *ad hoc* aid in the calculations rather than by tedious and unnecessary self-consistency conditions. As by Eq. (2) the *exact* $\bar{G}_{nm}(z)$ are all independent of $\Sigma(z)$, in any *accurate approximation* to $\bar{G}_{nm}(z)$ we have latitude in our choice of $\Sigma(z)$, as discussed below, and we pick the simplest possible $\Sigma(z)$ for which our calculated G is approximately stationary.

We next define a modified resolvent operator $G^{(i)}$ appropriate to the case in which one sets $\tilde{V}_i = 0$, where we define $\tilde{V}_i \equiv \langle i \,|(V-\Sigma)_i\,| i\rangle$ and, indicating the elimination of the localized fluctuation potential at this site by $(\ )_i'$, we have

$$G^{(i)}(z) \equiv [z - (T+\Sigma) - (V-\Sigma)_i']^{-1}. \tag{4}$$

The full resolvent (2) can be expressed in terms of the modification in (4) by the use of the operator identity $(A-B)^{-1} = A^{-1} + A^{-1}B(A-B)^{-1}$:

$$G(z) = G^{(i)}(z) + G^{(i)}(z)(V-\Sigma)_i G(z). \tag{5}$$

Because the perturbation is diagonal in the Wannier representation, the matrix elements are easily found:

$$G_{nm}(z) = G^{(i)}_{nm}(z) + G^{(i)}_{ni}(z)\tilde{V}_i G^{(i)}_{im}(z)/(1 - G^{(i)}_{ii}(z)\tilde{V}_i). \tag{6}$$

For the calculation of the density-of-states function $\rho(\omega) \equiv (-1/\pi)\,\mathrm{Im}\bar{G}_{nn}(\omega + i\epsilon)$ only the configurationally averaged Green's function $\bar{G}_{nn}(\omega+i\epsilon)$ is required. For the one-particle propagators $\bar{G}_{\vec{k}\vec{k}}$ the averaged Fourier transforms of all $\bar{G}_{nm}(\omega+i\epsilon)$ are needed. Equation (6) is now iterated. Define $\bar{G}^{(i,j)}(z)$ to be the modified resolvent operators with the fluctuation potentials $\tilde{V}$ at sites i and j removed. By a repetition of the above, we have

$$G^{(i)}_{nm}(z) = G^{(i,j)}_{nm}(z) + G^{(i,j)}_{nj}\tilde{V}_j G^{(i,j)}_{jm}/(1 - G^{(i,j)}_{jj}\tilde{V}_j). \tag{7}$$

The matrix elements G_{nm} decay exponentially with distance R_{nm}; thus the expansions (6) and (7) are in a symbolic "parameter" γ defined as $G^{(\cdots)}_{nj}\tilde{V}_j$, which is "small" for small $\tilde{V}_j$ and "exponentially small" at large $\tilde{V}_j$. *The processes (6) and (7) are to be repeated any number of times, until the largest practical cluster size is achieved.*[10] Termination, by truncation, of the series consists of approximating the most distant G's, i.e., those with the largest number of superscripts, by their value in the average optical potential. Thus, if we stop at (7), the approximation consists in replacing $G^{(i,j)}_{nm}(z)$ by $\langle n\,|[z-(T+\Sigma)]^{-1}|m\rangle$. The configurational averages over all the explicitly retained V_i are then performed, and all $\bar{G}$'s obtained.

III. CHOICE OF Σ

We now come to our principal point of departure from other methods—our choice of Σ. Our results would depend crucially upon Σ except for the following observations. Since the behavior of the local cluster is the dominant characteristic of disordered systems, we expect results insensitive to the particular choice of Σ if the cluster size is sufficiently large.

We require a simple functional form for Σ that allows for states out to the bands limits. This excludes the use of Σ_{CPA} which is known to produce bands that are always too narrow. We restrict the range of possible Σ's by requiring that it obey dispersion relations, insuring that our approximate G is analytic. Furthermore, a functional form is desired in which G is accurate in both the weak as well as strong scattering regimes. Because of the local nature of highly disordered systems, our choice becomes more critical for small potential differences where effects are more extended. Our input is the $\mathrm{Im}\Sigma$ which we take as one or more step functions, nonzero only within the theoretical band limits. $\mathrm{Re}\Sigma$ is then determined from the following dispersion relation:

$$\Sigma(z) = \tfrac{1}{2}\langle V\rangle + \frac{1}{2\pi i}\int_{-\infty}^{\infty} dx\,\frac{\Sigma(x+i\epsilon)}{x-z}. \tag{8}$$

This is sufficient to make our approximation to $G(z)$ satisfy causality. The density-of-states sum rule, $\int_{-\infty}^{\infty} d\omega\,\rho(\omega) = 1$ is itself a beneficial consequence of the analyticity of our approximate $G(z)$ and its resulting $1/z$ dependence in the asymptotic limit as we discuss elsewhere.[11] We verified that in all cases studied, the sum rule on $\rho(\omega)$ was satisfied numerically. If we choose the constant $\mathrm{Im}\Sigma$ to be of magnitude of $\mathrm{Im}\Sigma_{\mathrm{CPA}}$, then in the weak-scattering and low-concentration regimes $G(z)$ will be quite similar to $G_{\mathrm{CPA}}(z)$ so that accurate results can be expected in all regimes.

Before we proceed, the way in which we use $\mathrm{Im}\Sigma_{\mathrm{CPA}}$ must be more clearly outlined. In the accompanying Fig. 1 we display the two basic behavior patterns of $|\mathrm{Im}\Sigma_{\mathrm{CPA}}|$ as observed by Velický, Kirkpatrick, and Ehrenreich.[12] It should be noted that, here also, $\mathrm{Re}\Sigma$ and $\mathrm{Im}\Sigma$ are related by the Eq. (8). Σ has to describe everything in the CPA; it determines band gaps, peaks in the density of states, and the general overall scale. Most of these results (e.g., band gaps and complicated structure) are better obtained by our detailed calculations of the correlated scattering. We hypothesize that the most useful information from CPA is contained in the general overall magnitude of $\mathrm{Im}\Sigma_{\mathrm{CPA}}$. Operationally, in Fig. 1(a), we would ignore values of $|\mathrm{Im}\Sigma_{\mathrm{CPA}}|$ from the region of its maximum as well as the extremeties of the band. In the former range of energies, we expect exceptional scattering because it is easiest for these states to make transitions due to band overlap, whereas at the band edges the spectrum will be least disturbed, according to the same considerations. Any value from the shaded region is then acceptable. In terms of particle lifetimes, we will obtain the large and small transition rates be-

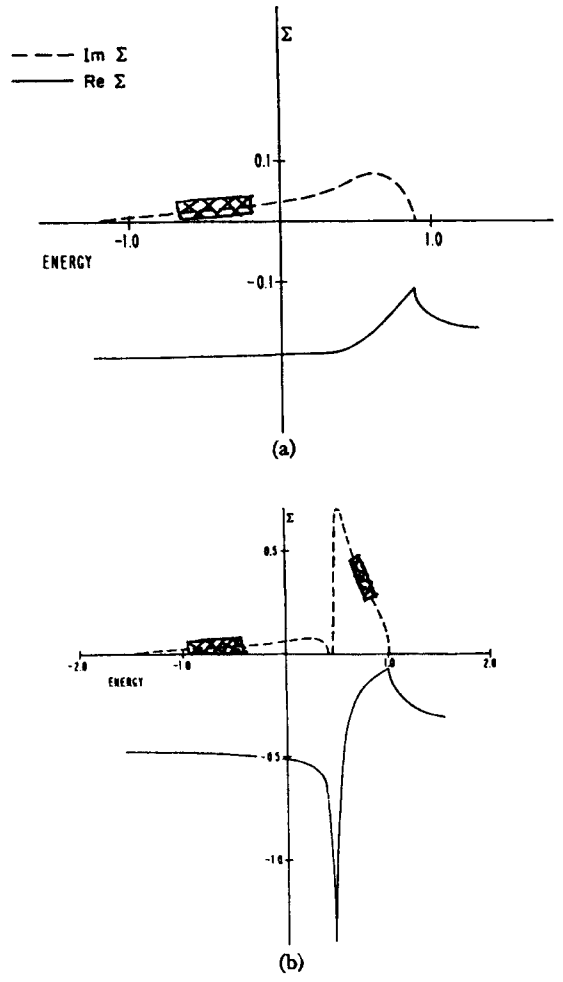

FIG. 1. Real and imaginary parts of the complex self-energy in the CPA. The two sets of curves are indicative of the type of results that can be expected from this approximation. (a) A situation where the alloy bands overlap; (b) the case of split bands. Energy is in units of half-bandwidth. This is an adaption of a figure from Ref. 12.

cause we almost solve the eigenvalue problem exactly for each configuration and this is clearly equivalent to a perturbation approach. As for concentration dependence in Σ_{CPA}, we will obtain correct behavior simply because we weigh each configuration by its appropriate probability. Thus we are able to include both the dynamical and statistical aspects of the problem.

In Fig. 1(b), the same analysis leads us to ignore the very large values of $|\mathrm{Im}\Sigma_{CPA}|$ in both subbands. Here though, the magnitudes are considerably different leading us to suspect that two different constants are needed. Further details of this case will be elucidated in the following examples.

IV. ANALYSIS OF RESULTS

We first consider the canonical one-dimensional tight-binding binary alloy for three different scattering strengths at a 50-50 concentration. Figure 2 compares the results of one-, three-, and five-cluster calculations for $\rho(\omega)$ when $V_i = \pm 0.5$ with exact results. We see in this example the development of the peaky structure associated with special clusters of atoms as our cluster size increases. Proceeding to a larger scattering strength ($V_i = \pm 1.0$), we expect that the local configurations will play a more prominent role because of increased wave function localization. As shown in Fig. 3 we successfully reproduce most of the structural details of $\rho(\omega)$ for a five cluster. To check the degree of insensitivity in our five-cluster model we varied $|\mathrm{Im}\Sigma|$ within the limits given by $\mathrm{Im}\Sigma_{CPA}$ and found little change in the overall pattern as shown in Fig. 4. This indicates, numerically that the resulting G is stationary and that Σ is optimum.

The scattering strengths are now increased to $V_i = \pm 2.0$, providing a critical evaluation of the methods capabilities (larger scattering strengths

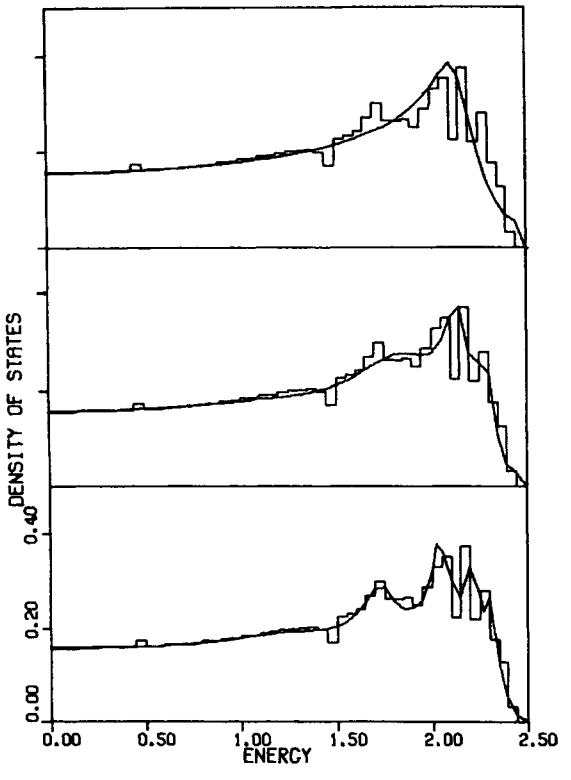

FIG. 2. Comparison of one-, three-, and five-cluster calculations for $\rho(\omega)$ using $|\mathrm{Im}\Sigma_{trial}| = 0.15$, with $V_i = \pm 0.5$, $c = 0.5$. Background (histogram) is exact results of Ref. 4. Energy is in units of half-bandwidth.

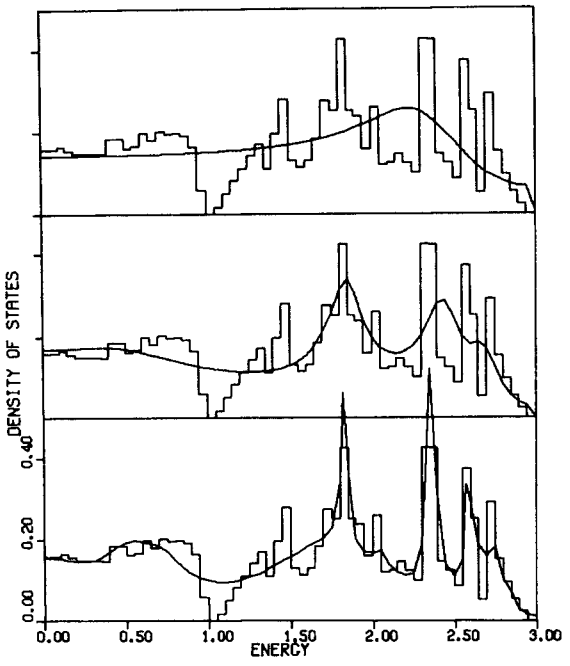

FIG. 3. Comparison of one-, three-, and five-cluster calculations for $\rho(\omega)$ in one dimension using $|\mathrm{Im}\Sigma_{\mathrm{trial}}| = 0.5$, with $V_i = \pm 1.0$ and $c = 0.5$. Background (histogram) is exact results of Ref. 4. Energy is in units of half-bandwidth.

are in a sense too easy because wave function localization makes a cluster calculation more plausible). Using the exact scattering off all configurations of five atoms, the highly discrete spectrum is well reproduced, as seen in Fig. 5(a). Increasing the cluster size to seven atoms, keeping the convergence factor the same as in Fig. 5(a), improves our agreement with the exact results as shown in Fig. 5(b). In Fig. 6 we display the results of again varying $|\mathrm{Im}\Sigma|$ within the limits dictated by $\mathrm{Im}\Sigma_{\mathrm{CPA}}$; the major details are again seen to remain stationary. We have found empirically that if $|\mathrm{Im}\Sigma|$ is too small, the resultant density of states is too "peaky" and as such, representative of a molecular cluster, instead of the solid state. If $|\mathrm{Im}\Sigma|$ is too large, then the central site predominates, as is correct only in the extreme "atomic" limit when potential fluctuations greatly exceed the bandwidth. One can see this from Fig. 6 since the sharper curve is associated with the lowest value of $|\mathrm{Im}\Sigma|$ and vice versa.

In three dimensions the obvious cluster size is seven sites. Figure 7 compares our calculation with the Monte-Carlo-type numerical results of Alben *et al.*[13] A constant $\mathrm{Im}\Sigma$ gave poor results in this case, but the CPA calculations immediately showed us why: $\mathrm{Im}\Sigma_{\mathrm{CPA}}$ was more than one order of magnitude smaller in the majority subband than in the minority subband. Consequently we changed $\mathrm{Im}\Sigma$ to the step function shown in the figure, varying the parameters (magnitudes of the steps) again guided by CPA. The results now agreed well with the exact computations and were insensitive to the precise value of our parameters as is evidenced by Fig. 8 in which a three-step function was used.

To illustrate entirely new applications, consider effects of short-range order on this same alloy. With α the Cowley short-range order parameter—c_A and $c_B = 1 - c_A$ the relative concentrations and P_{AB} the probability of finding atom A at a given site when a B atom occupies a specified neighboring site—we have $P_{AA} = c_A + c_B\alpha$, $P_{BA} = c_B(1-\alpha)$, $P_{AB} = c_A(1-\alpha)$, and $P_{BB} = c_B + c_A\alpha$. In Ref. 13, $\alpha = 0$. For $c_A = 0.1$, α can vary from -0.11 to $+1.0$; negative α is associated with enhanced tendency of A atoms to be surrounded by B's (i.e., "antiferromagnetism"), positive α indicates enhancement in the probability of either species being surrounded by atoms of its own kind (i.e., "ferromagnetism"). Using the same convergence parameters as in our calculation at $\alpha = 0$, in Fig. 9 we find distinctive features in the minority subband

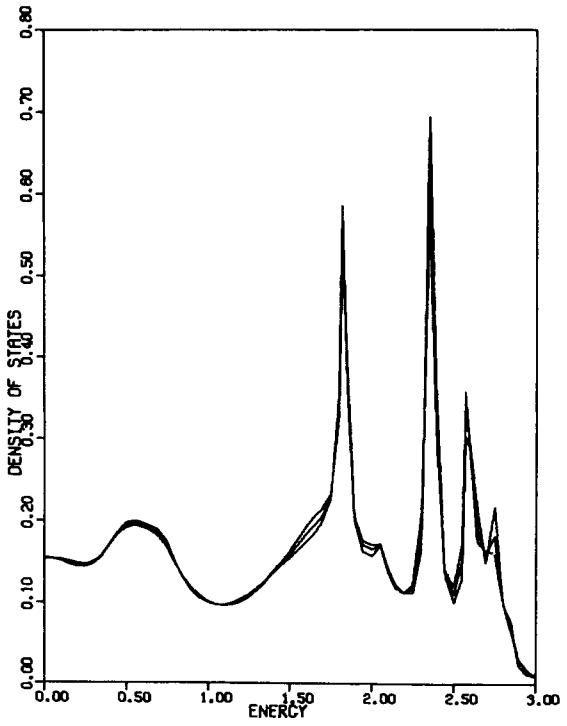

FIG. 4. Curves give $\rho(\omega)$ for three different values of Σ_{trial} for a five-cluster calculation of a one-dimensional alloy with $V_i = \pm 1.0$ and $c = 0.5$. The sharpest peaks are associated with lowest value of $|\mathrm{Im}\Sigma_{\mathrm{trial}}|$, 0.4. Other values are 0.5 and 0.6. Energy is in units of half-bandwidth.

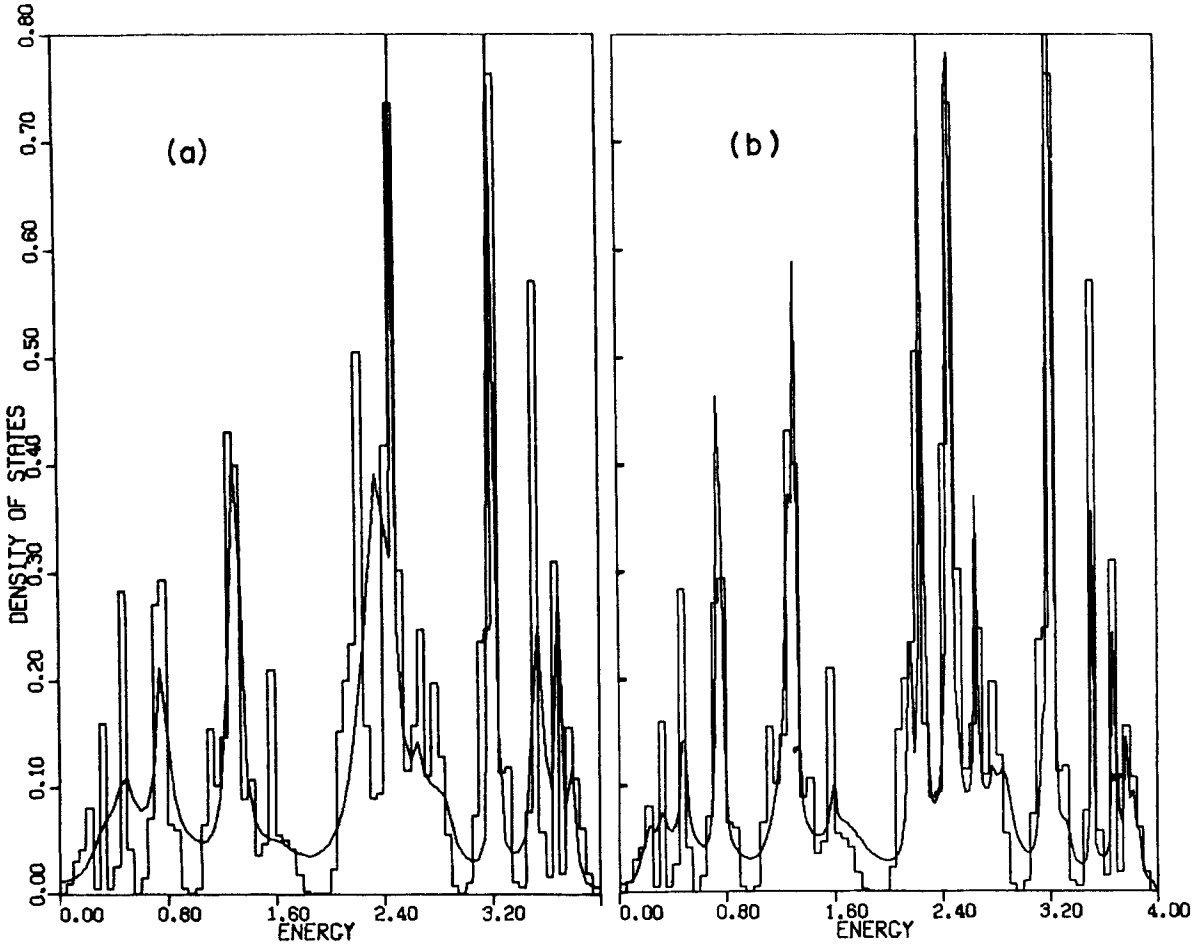

FIG. 5. (a) Density of states for a (50–50)% concentration one-dimensional alloy with $V_A=2.0$, $V_B=-2.0$. Histogram is exact calculations from Ref. 4. The full band is obtained by reflecting the portion shown through the origin. These results were computed from $\mathrm{Im}\Sigma=-0.80$ and $\mathrm{Re}\Sigma$ obtained from $\mathrm{Im}\Sigma$ by Eq. (8), including the exact scattering from all configurations of a central atom and its four nearest neighbors. (b) Extension of the above results to a cluster of seven atoms using the same $\Sigma(\omega)$. This result is comparable in accuracy and wealth of detail to the best self-consistent calculation to date, Ref. 4. Energy is in units of half-bandwidth.

density of states that we interpret in terms of minority-atom clustering: the single peak of $\alpha = -0.07$ registers the unlikelihood of finding two A atoms as nearest neighbors, and the double peaks of $\alpha = 0.7$ represent the tendency of the same atoms to form pairs, triplets, etc. However, due to the sparseness of A atoms, triplets and higher-order clusters are statistically insignificant for these values of α.

V. ELECTRON PROPAGATION

So far we have developed a method for calculating the site-diagonal configuration averaged Green's function. We have not indicated, how we would calculate the non-site-diagonal propagators. One alternative is to develop a cluster method for the latter, similar to the method we used for the former. Another, simpler though less accurate, alternative will be employed. We first define a new self-energy $\Lambda^*(z)$ by the equation

$$\bar{G}_{ll}(z) \equiv \frac{1}{N}\sum_{\vec{k}} \frac{1}{z - \Lambda^*(z) - \epsilon_{\vec{k}}}. \tag{9}$$

This relationship is numerically inverted to obtain Λ^* as a function of the exact or numerically calculated $\bar{G}_{ll}$. From the calculation of $\Lambda^*(\omega)$ we obtain $\Lambda^*(z)$ in the entire complex plane as

$$\Lambda^*(z) = \langle V\rangle + \frac{1}{\pi}\int_{-\infty}^{\infty} d\omega \frac{\mathrm{Im}\Lambda^*(\omega + i\epsilon)}{\omega - z}. \tag{10}$$

If further values of $\bar{G}_{lm}(z)$ were calculated numer-

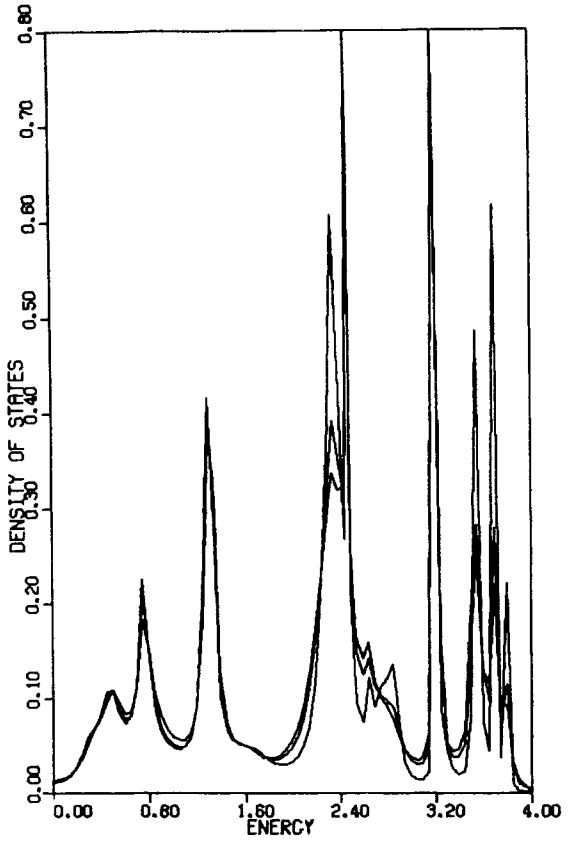

FIG. 6. Curves give $\rho(\omega)$ for three different values of Σ_{trial} for a five-cluster calculation of a one-dimensional alloy with $V_i = \pm 2.0$ and $c = 0.5$. The sharpest peaks are associated with lowest value of $|\text{Im}\Sigma_{\text{trial}}| = 0.4$, other values are 0.8 and 1.0. Energy is in units of half-bandwidth.

ically, then we would determine $\Lambda^*(\vec{k}, z)$ from

$$\bar{G}_{lm}(z) \equiv \frac{1}{N} \sum_{\vec{k}} \frac{e^{i\vec{k}\cdot(\vec{R}_l - \vec{R}_m)}}{z - \Lambda^*(\vec{k}, z) - \epsilon_{\vec{k}}} \tag{11}$$

and

$$\bar{G}_{\vec{k}\vec{k}} = [z - \Lambda^*(\vec{k}, z) - \epsilon_{\vec{k}}]^{-1} .$$

The analysis is facilitated by going over to a localized representation in which we would specify the number of elements $\Lambda^*_{lm}(z)$ that we have determined numerically. For example, if we have available $\bar{G}_{l,l}(z)$, $\bar{G}_{l,l+1}(z)$, and $\bar{G}_{l,l+2}(z)$, then we would be able to obtain

$$\Lambda^*_{l,m}(z) = \delta_{l,m}\Lambda^*_0(z) + \delta_{l+1,m}\Lambda^*_1(z) + \delta_{l+2,m}\Lambda^*_2(z) ,$$

by solving the three equations simultaneously. In the case at hand, we will use a site-diagonal self-energy since all we have at our disposal are the computed $\bar{G}_{ll}(z)$. We will still use

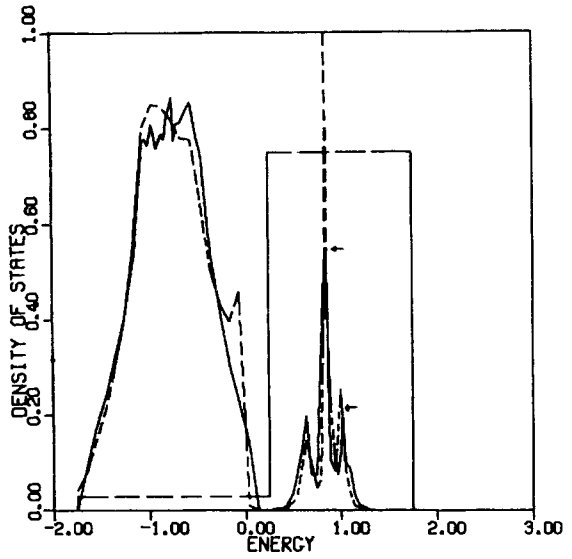

FIG. 7. Comparison of seven-cluster calculations of $\rho(\omega)$ (dashed line) using a two-step $|\text{Im}\Sigma_{\text{trial}}|$ (long dashed line), with numerical work of Alben *et al.* (Ref. 13) (solid line) who solved the Schrödinger equation for an 8000-atom three-dimensional tight-binding solid. The potentials are $V_i = \pm 0.75$ with impurity concentration of 0.1. Small horizontal arrows indicate the height to which their peaks rise. Energy is in units of half-bandwidth.

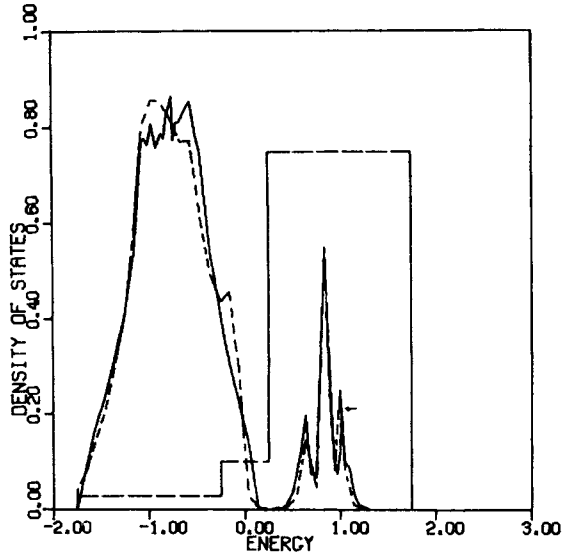

FIG. 8. Comparison of seven-cluster calculation of $\rho(\omega)$ (dashed line) using a three-step $|\text{Im}\Sigma_{\text{trial}}|$ (long dashed line) with results of Alben *et al.* (Ref. 13) (solid line). $V_i = \pm 0.75$ and $c = 0.1$ for this three-dimensional tight-binding alloy. The sharp peak in Fig. 7 at $\omega = 0.86$ is absent because of the coarser energy scale used. Arrow indicates the height to which their peak rises. Energy is in units of half-bandwidth.

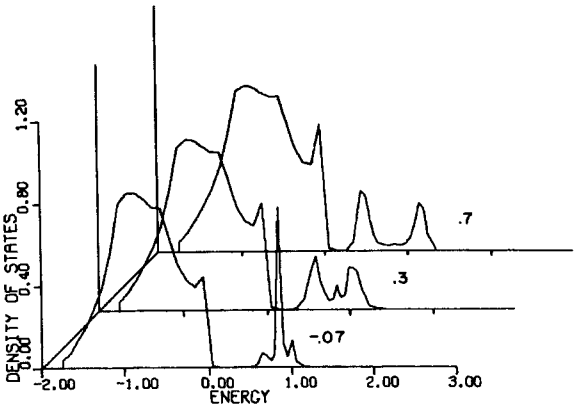

FIG. 9. Density of states for $V_A=0.75$, $V_B=0.75$ in a three-dimensional simple cubic lattice with concentration $c_A=0.1$. Cowley short-range order parameter α is -0.07, 0.3, and 0.7, respectively. $|\mathrm{Im}\Sigma|$ is the same as in Fig. 7 (dot-dash line) and $\mathrm{Re}\Sigma$ is obtained therefrom by use of Eq. (8). Energy is in units of half-bandwidth.

$$\bar{G}_{lm}(z)=\frac{1}{N}\sum_{\vec{k}}\frac{e^{i\vec{k}\cdot(\vec{R}_l-\vec{R}_m)}}{z-\Lambda^*(z)-\epsilon_{\vec{k}}},$$

hence (12)

$$\bar{G}_{\vec{k}\vec{k}'}=[z-\Lambda^*(z)-\epsilon_{\vec{k}}]^{-1},$$

as the definition of the off-diagonal elements. The propagators decay rapidly with distance R_{lm} so both the one-, two-, or three-point curve-fitting procedures will probably give reasonably equivalent results. Now, all the information contained in our previous numerical work is stored in $\Lambda^*(z)$, the complex proper self-energy part. It is of interest to compare $\mathrm{Im}\Lambda^*$ with $\mathrm{Im}\Sigma_{\mathrm{CPA}}$ in order to see how they differ. This is done in Fig. 10 for the one-dimensional alloy of Figs. 5 and 6.

In summary we have presented a relatively simple method for calculating the eigenvalue spectrum of a disordered system, one that avoids all the computational pitfalls of self-consistent methods. This quasi-invariant theory is not only highly accurate, but also allows the bounds on the frequency spectrum to be naturally determined by the correlated scattering of a local group. We now discuss transport and develop a formalism that allows our numerical output to be used in approximations that conserve particle number and energy.

VI. TRANSPORT IN DISORDERED SYSTEMS

The linear response of the current to the electric field defines the conductivity, which we take to be the same along the three principal directions in our simple cubic structure. Following Velický[14] we have in our single-particle model

$$\sigma(0)=\frac{\pi}{m^2}\int_{-\infty}^{\infty}d\lambda\left(-\frac{\partial f(\lambda)}{\partial\lambda}\right)\langle\langle\delta(\lambda-H)p_1\delta(\lambda-H)p_1\rangle\rangle, \tag{13}$$

where e, the electric charge, is unity and f is the fermi function. The bracketed term is short hand for

$$\langle\langle\delta(\lambda-H)p_1\delta(\lambda-H)p_1\rangle\rangle \equiv\sum_{\alpha}\langle\langle\alpha\,|\,\delta(\lambda-H)p_1\delta(\lambda-H)p_1\,|\,\alpha\rangle\rangle. \tag{14}$$

p_1 is the momentum operator along an arbitrarily chosen principal axis and $\langle\ \rangle$ denotes configuration averaging. Examination of Eq. (14) reveals that we require the two-particle correlation function

$$\langle G^2_{imjl}(z_1,z_2)\rangle=\langle\langle i\,|\,(z_1-H)^{-1}\,|\,j\rangle\langle m\,|\,(z_2-H)^{-1}\,|\,l\rangle\rangle. \tag{15}$$

We can relate $\langle G^2\rangle$ to $\bar{G}$ by the equation

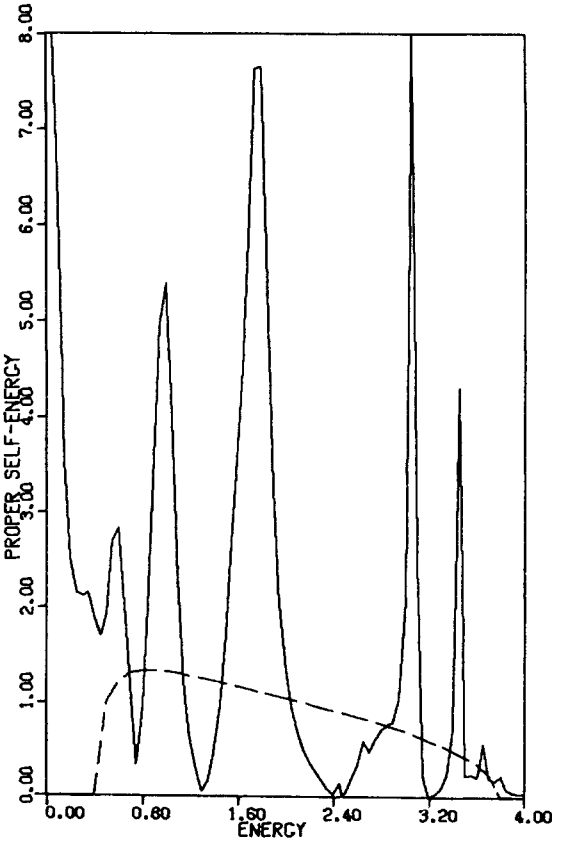

FIG. 10. Solid line is $|\mathrm{Im}\Lambda^*(\omega)|$ for the one-dimensional alloy of Figs. 5 and 6 in the five-cluster approximation while the dashed line is the corresponding $|\mathrm{Im}\Sigma_{\mathrm{CPA}}(\omega)|$. Energy is in units of half-bandwidth.

$$\langle G^2_{imjl}(z_1,z_2)\rangle = \overline{G}_{ij}(z_1)\overline{G}_{ml}(z_2) + \sum_{\substack{kp\\qr}} \overline{G}_{ik}(z_1)\,\overline{G}_{ql}(z_2)\Xi_{kr,pq}\langle G^2_{pmjr}(z_1,z_2)\rangle\,, \tag{16}$$

which defines the index structure of the vertex function. This equation is exact for the exact $\overline{G}$ and we will use it to define $\langle G^2\rangle$ when we have an approximate single-particle Green's function. We can place restrictions on possible vertex functions by requiring the conservation of charge and energy in the presence of a long-wavelength disturbance. This leads to the introduction of a new operator

$$K(z_1,z_2) = \langle (z_1 - H)^{-1}(z_2 - H)^{-1}\rangle\,. \tag{17}$$

It is easy to show that K must satisfy the following Ward-type identity:

$$K(z_1,z_2) = (z_2 - z_1)^{-1}[\overline{G}(z_1) - \overline{G}(z_2)]\,, \tag{18}$$

which implies a connection between the one-body operator $\overline{G}$ and the two-body Green's function $\langle G^2\rangle$. Also, one can show with the above condition that the linear response of the particle number and energy to a long-wavelength disturbance is zero, thus ensuring the appropriate conservation laws. If we use an approximate $\overline{G}$, then we must construct a K that maintains Eq. (18) and this allows us to relate $\overline{G}$ to the vertex function in the following way: We let $z_2 \to z_1$, then Eq. (18) becomes

$$K_{il}(z_1,z_1) = -\frac{d\overline{G}_{il}(z_1)}{dz_1}\,. \tag{19}$$

The configuration averaged resolvent can be written

$$\overline{G}_{il}(z_1) = \langle i\,|\,[z_1 - T - \Lambda^*_{op}(z_1)]^{-1}\,|\,l\rangle\,, \tag{20}$$

which leads to the equation

$$K_{il}(z_1,z_1) = \sum_j \overline{G}_{ij}(z_1)\overline{G}_{jl}(z_1) + \sum_{kq} \overline{G}_{ik}(z_1)\left(\frac{-d\Lambda^*_{kq}(z_1)}{dz_1}\right)\overline{G}_{ql}(z_1)\,. \tag{21}$$

But

$$\frac{-d\Lambda^*_{kq}(z_1)}{dz_1} = \frac{1}{N}\sum_{rp}\frac{d\Lambda^*_{kq}(z_1)}{d\overline{G}_{pr}(z_1)}\left(\frac{-d\overline{G}_{pr}(z_1)}{dz_1}\right) = \frac{1}{N}\sum_{rp}\frac{d\Lambda^*_{kq}(z_1)}{d\overline{G}_{pr}(z_1)}K_{pr}(z_1,z_1)\,,$$

so that

$$K_{il}(z_1,z_1) = \sum_j \overline{G}_{ij}(z_1)\overline{G}_{jl}(z_1) + \sum_{\substack{kq\\rp}} \overline{G}_{ik}(z_1)\overline{G}_{ql}(z_1)\frac{1}{N}\frac{d\Lambda^*_{kq}(z_1)}{d\overline{G}_{pr}(z_1)}K_{pr}(z_1,z_1)\,. \tag{22}$$

In $\langle G^2\rangle$, we let $m = j$ and sum over all j with $z_1 = z_2$:

$$\sum_j \langle G^2_{ijjl}(z_1,z_1)\rangle = \sum_j \overline{G}_{ij}(z_1)\overline{G}_{jl}(z_1) + \sum_{\substack{kq\\rp}} \overline{G}_{ik}(z_1)\overline{G}_{ql}(z_1)\Xi_{kr,pq}(z_1,z_1)\sum_j \langle G^2_{pjjr}(z_1,z_1)\rangle\,. \tag{23}$$

Once we recognize

$$K_{il}(z_1,z_1) = \sum_j \langle G^2_{ijjl}(z_1,z_1)\rangle\,,$$

we find that the vertex must satisfy the equation

$$\Xi_{kr,pq}(z_1,z_1) = \frac{1}{N}\frac{d\Lambda^*_{kq}(z_1)}{d\overline{G}_{pr}(z_1)}\,. \tag{24}$$

We note that not only must this relationship hold for the exact vertex function and self-energy but also in any approximation in which it is desired that the two-particle correlation function satisfy the Ward identity, Eq. (18). This means that once an approximation is made to Λ^*, we can determine transport functions that allow the conservation laws to be obeyed. We could make further approximations to $\langle G^2\rangle$ but we would then have no guarantee of conserving charge, energy, etc. The Ward identity is useful to generate a unique compatible vertex function only when the frequencies are the same. For the case at hand, $\Lambda^*_{kq}(z_1) = \delta_{kq}\Lambda^*(z_1)$ is a function of the site-diagonal averaged Green's function so the vertex is

$$\Xi_{kr,pq}(z_1,z_1) = \frac{\delta_{kq}\delta_{rp}}{N}\frac{d\Lambda^*(z_1)}{d\overline{G}_{rr}(z_1)} = \delta_{kq}\delta_{rp}\Xi(z_1,z_1)\,. \tag{25}$$

For $z_1 \neq z_2$, we make the approximation

$$\Xi_{kr,pq}(z_1,z_2) = \delta_{kq}\delta_{rp}\Xi(z_1,z_2)\,. \tag{26}$$

This is certainly consistent with the Ward identity, and furthermore, it allows us to show that contributions to the conductivity from the vertex corrections then vanish. The two-particle correlation function is now

$$\langle G^2_{imjl}(z_1,z_2)\rangle = \bar{G}_{ij}(z_1)\bar{G}_{ml}(z_2) + \sum_k \bar{G}_{ik}(z_1)\bar{G}_{kl}(z_2)\Xi(z_1,z_2)\sum_r \langle G^2_{rmjr}(z_1,z_2)\rangle . \tag{27}$$

To find the conductivity we need $\langle\langle \delta(\lambda_1 - H)p_1\delta(\lambda_2 - H)p_2\rangle\rangle$ or

$$I_{12}(\lambda_1,\lambda_2) = \sum_{ijlm} p^{\vec{1}}_{jm}\langle\langle m\,|\,\delta(\lambda_2 - H)\,|\,l\rangle\rangle p^{\vec{2}}_{li}\langle\langle i\,|\,\delta(\lambda_1 - H)\,|\,j\rangle\rangle , \tag{28}$$

which requires

$$\sum_{ijlm} p^{\vec{1}}_{jm}p^{\vec{2}}_{li}\langle G^2_{imjl}(\lambda_1,\lambda_2)\rangle = \sum_{ijlm} p^{\vec{1}}_{jm}p^{\vec{2}}_{li}\bar{G}_{ij}(\lambda_1)\bar{G}_{ml}(\lambda_2) + \sum_{ijlm}\sum_k p^{\vec{2}}_{li}\bar{G}_{ik}(\lambda_1)\bar{G}_{kl}(\lambda_2)\Xi(\lambda_1,\lambda_2)\sum_r \langle G^2_{rmjr}(\lambda_1,\lambda_2)\rangle p^{\vec{1}}_{jm} . \tag{29}$$

The second term breaks up into

$$\sum_{ilk} p^{\vec{2}}_{li}\bar{G}_{ik}(\lambda_1)\bar{G}_{kl}(\lambda_2)\sum_{jmr}\Xi(\lambda_1,\lambda_2)\langle G^2_{rmjr}(\lambda_1,\lambda_2)\rangle p^{\vec{1}}_{jm} \equiv AB . \tag{30}$$

Let us transform the Wannier sum in A to a Bloch sum. Then since $\langle\vec{k}\,|\,p_2\,|\,\vec{k}'\rangle = mV_2(\vec{k})\delta_{\vec{k}\vec{k}'}$, and $\bar{G}$ is diagonal in the Bloch representation,

$$A = m\sum_{\vec{k}} V_2(\vec{k})\bar{G}_{\vec{k}\vec{k}}(\lambda_1)\bar{G}_{\vec{k}\vec{k}}(\lambda_2) = m\sum_{\vec{k}}\frac{\partial\epsilon_{\vec{k}}}{\partial k_2}\,\frac{1}{\lambda_1 - \Lambda^*(\lambda_1^+) - \epsilon_{\vec{k}}}\,\frac{1}{\lambda_2 - \Lambda^*(\lambda_2^+) - \epsilon_{\vec{k}}} . \tag{31}$$

The propagators are even under inversion ($\vec{k}\to -\vec{k}$) but the velocity $V_2 = \partial\epsilon/\partial k_2$ is odd, giving us zero, and all vertex corrections now vanish. In this case, the fortunate cancellation of vertex corrections comes about as a consequence of the approximation of the proper self-energy by a site-diagonal quantity, Eq. (12).

VII. ZERO-TEMPERATURE dc CONDUCTIVITY

We are now in a position to evaluate $\sigma(0)$. Because the vertex corrections vanish,

$$I_{12}(\lambda,\lambda) = \sum_{ijlm} p^{\vec{1}}_{jm}\langle\langle m\,|\,\delta(\lambda - H)\,|\,l\rangle\rangle p^{\vec{2}}_{li}\langle\langle i\,|\,\delta(\lambda - H)\,|\,j\rangle\rangle = m^2\sum_{\vec{k}} V_1(\vec{k})V_2(\vec{k})\langle\langle\vec{k}\,|\,\delta(\lambda - H)\,|\,\vec{k}\rangle\rangle^2 . \tag{32}$$

With the definition

$$\langle\langle\vec{k}\,|\,\delta(\lambda - H)\,|\,\vec{k}\rangle\rangle = (-1/\pi)\,\mathrm{Im}\bar{G}_{\vec{k}\vec{k}}(\lambda^+),$$

we get for $\vec{1} = \vec{2}$ $[\sigma(\omega) = \sigma_{11}(\omega)]$,

$$\sigma(0) = \frac{2}{\pi}\int_{-\infty}^{\infty} d\lambda\left(\frac{-\partial f(\lambda)}{\partial\lambda}\right) \times \sum_{\vec{k}} V_1(\vec{k})^2[\mathrm{Im}\bar{G}_{\vec{k}\vec{k}}(\lambda^+)]^2 , \tag{33}$$

where we have included a factor of 2 for the two possible spin orientations. At $T = 0$, $-\partial f(\lambda)/\partial\lambda = \delta(\lambda - \mu)$, with μ the chemical potential, and the conductivity per atom is

$$\sigma(0) = \frac{2}{\pi N}\sum_{\vec{k}} V_1(\vec{k})^2[\mathrm{Im}\bar{G}_{\vec{k}\vec{k}}(\mu^+)]^2 \tag{34}$$

or

$$\sigma(0) = \frac{2}{\pi}\int_{-\infty}^{\infty} dE\left(\frac{\mathrm{Im}\Lambda^*(\mu^+)}{[\mu - \mathrm{Re}\Lambda^*(\mu^+) - E]^2 + \mathrm{Im}\Lambda^*(\mu^+)^2}\right)^2 \times\frac{1}{N}\sum_{\vec{k}} V_1(\vec{k})^2\delta(E - \epsilon_{\vec{k}}) . \tag{35}$$

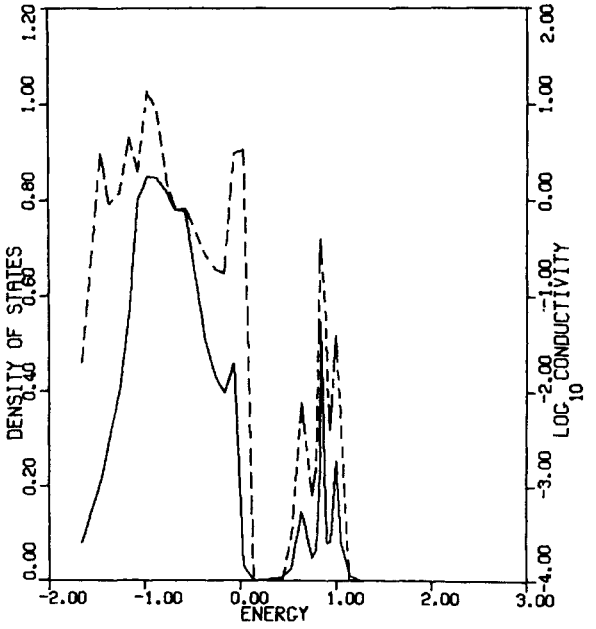

FIG. 11. Then dc conductivity (dashed line) of a three-dimensional alloy with $V_i = \pm 0.75$ and $c = 0.1$. Density of states taken from Fig. 7 is shown in the solid line. Energy is in units of half-bandwidth.

This natural separation, only possible for a proper self-energy independent of $\vec{k}$, isolates the lifetime and energy shifts of the single-particle excitations from that part of the conductivity which pertains to the particular lattice under study. We will concentrate on a three-dimensional simple cubic lattice with

$$\epsilon_{\vec{k}} = \tfrac{1}{3}(\cos k_x + \cos k_y + \cos k_z) .$$

Then,

$$V_1(\vec{k})^2 = \tfrac{1}{9}\sin^2 k_x = \tfrac{1}{9}(1 - \cos^2 k_x) .$$

Consider the functions

$$P_n(E) \equiv \frac{1}{N}\sum_{\vec{k}} \frac{e^{nik_x}}{E - \epsilon_{\vec{k}}} ,$$

for which we have

$$\frac{1}{N}\sum_{\vec{k}} V_1(\vec{k})^2 \delta(E - \epsilon_{\vec{k}}) = \frac{1}{18\pi}\,\mathrm{Im}[P_2(E^+) - P_0(E^+)] .$$

The imaginary part of both $P_2(E^+)$ and $P_0(E^+)$ vanish outside the unperturbed band and

$$\sigma(0) = \frac{1}{9\pi^2}\,\mathrm{Im}\int_{-1}^{1} dE \left(\frac{\mathrm{Im}\Lambda^*(\mu^+)}{[\mu - \mathrm{Re}\Lambda^*(\mu^+) - E]^2 + \mathrm{Im}\Lambda^*(\mu^+)^2}\right)^2 [P_2(E^+) - P_0(E^+)] . \tag{36}$$

We have calculated the dc conductivity for our three-dimensional alloy in order to illustrate our formal results. Generally, there are two ways in which the dc conductivity can vanish. If the density of states at the Fermi level is zero then so is $\sigma(0)$. In addition, we can have a finite $\rho(\mu)$, but a zero mobility because of wave-function localization. Equation (36) only admits a zero in $\sigma(0)$ if $\rho(\mu)$ is zero so we cannot take the latter possibility into account. The conductivity is displayed in Fig. 11 against its respective density of states. There is a rather direct correlation between the magnitude of the density of states and that of the conductivity. This relationship is understood in terms of the availability of states at a given energy to which an initial state can make a transition. We also find peaks in $\sigma(0)$ which we associate with velocity peaks in the cubic band structure.

*Supported by AFOSR Grant No. 73-2430B.
†Research is supported by the ONR under Grant No. N00014-76-C-0690.

[1]R. J. Elliott, J. A. Krumhansl, and P. L. Leath, Rev. Mod. Phys. 46, 465 (1974); H. Ehrenreich and L. M. Schwartz, Solid State Phys. 31, 149 (1976); and J. D. Joannopoulos and Marvin L. Cohen, *ibid.* 31, 71 (1976).
[2]P. Soven, Phys. Rev. 156, 809 (1967); 178, 1136 (1969).
[3]D. W. Taylor, Phys. Rev. 156, 1017 (1967).
[4]W. H. Butler, Phys. Rev. B 8, 4499 (1973).
[5]Pabitra N. Sen and Felix Yndurain, Phys. Rev. B 13, 4387 (1976).
[6]R. Friedberg and J. M. Luttinger, Phys. Rev. B 12, 4460 (1975), and references cited therein.
[7]B. Velický, S. Kirkpatrick, and H. Ehrenreich, Phys. Rev. B 1, 3250 (1970).
[8]For example, while computer time increases exponentially with the number of neighboring shells over which one chooses to perform the exact configurational averages, the use of a Monte Carlo sampling technique may extend our calculations to large numbers of such shells at only a modest increase in computational time.
[9]G. Baym and L. Kadanoff, Phys. Rev. 124, 287 (1961).
[10]Our equations (6) and (7) were first derived by Vijay Kumar and S. J. Joshi [J. Phys. C 8, L148 (1975)] in the context of applying Butler's (Ref. 4) self-consistent equations to a tetrahedral alloy.
[11]A more complete exposition of this entire work is contained in the Ph.D. thesis of one of us (P.B.) (Yeshiva University, 1977) (unpublished).
[12]B. Velický, S. Kirkpatrick, and H. Ehrenreich, Phys. Rev. 175, 747 (1968).
[13]R. Alben, M. Blume, H. Krakauer, and L. Schwartz, Phys. Rev. B 12, 4090 (1975).
[14]B. Velický, Phys. Rev. 184, 614 (1969).